Available online at www.sciencedirect.com
ScienceDirect
Journal of Sound and Vibration 319 (2009) 1083–1096
JOURNAL OF SOUND AND VIBRATION
www.elsevier.com/locate/jsvi

# Numerical difficulties with boundary element solutions of interior acoustic problems

J.B. Fahnline

*The Applied Research Laboratory, Water Tunnel Building, University Park, PA 16802, USA*

Received 20 May 2007; received in revised form 1 May 2008; accepted 26 June 2008
Handling Editor: S. Bolton
Available online 20 August 2008

**Abstract**

Although boundary element methods have been applied to interior problems for many years, the numerical difficulties that can occur have not been thoroughly explored. Various authors have reported low-frequency breakdowns and artificial damping due to discretization errors. In this paper, it is shown through a simple example problem that the numerical difficulties depend on the solution formulation. When the boundary conditions are imposed directly, the solution suffers from artificial damping, which may potentially lead to erroneous predictions when boundary element methods are used to evaluate the performance of damping materials. This difficulty can be alleviated by first computing an impedance or admittance matrix, and then using its reactive component to derive the solution for the acoustic field. Numerical computations are used to demonstrate that this technique eliminates artificial damping, but does not correct errors in the reactive components of the impedance or admittance matrices, which then causes nonexistence and nonuniqueness difficulties at the interior resonance frequencies for hard-wall and pressure release boundary conditions, respectively. It is shown that the admittance formulation is better suited to boundary element computations for interior problems because the resonance frequencies for pressure release boundary conditions do not begin until the smallest dimension of the boundary surface is at least one half the acoustic wavelength. Aside from producing much more accurate predictions, the admittance matrix is also much easier to interpolate at low frequencies due to the absence of interior resonances. For the example problem considered, only the formulation using the reactive component of the admittance matrix produces accurate solutions as long as the surface element discretization satisfies the standard six-element-per-wavelength rule.


## 1. Introduction

In acoustics, boundary element methods were originally developed to solve exterior radiation problems. They are ideal for this type of problem because only the exterior boundary of the structure is discretized, rather than the entire solution domain. Boundary element methods can also be applied to interior acoustic problems, and are advantageous for geometrically complex boundaries or large acoustic domains. Common applications include computations of sound fields within passenger cabins of automobiles [1] and airplanes [2] and transmission loss calculations for mufflers [3,4] and silencers [5,6]. Damping materials are often included in the analysis using impedance boundary conditions.

*E-mail address:* jbf103@only.arl.psu.edu

0022-460X/$ - see front matter © 2008 Elsevier Ltd. All rights reserved.
doi:10.1016/j.jsv.2008.06.040

Interior and exterior boundary value problems in acoustics differ primarily because sound radiation to the farfield creates acoustic damping for exterior problems, whereas interior problems do not include damping unless impedance boundary conditions are specified with a nonzero resistive component. Without damping, the solution of the boundary value problem is not unique at the interior resonance frequencies for acoustic modes satisfying the homogeneous version of the specified boundary condition [7,8]. In theory, the acoustic field goes to infinity at the resonance frequencies when these modes are excited. In practice, the solution always remains finite in a numerical implementation due to discretization errors, and thus some level of error is expected near the response peaks.

In this paper, the main objective is to discuss what happens near the response peaks and to try to develop better methods for predicting the theoretical infinite response at resonance frequencies. The research was originally undertaken to try to explain obvious signs of artificial damping in boundary element computations of 4-pole parameters of water-filled pipes. A thorough literature search only yielded one reference to the subject by Langley [2], where it was theorized that artificial damping occurs in boundary element solutions due to discretization errors. Langley goes on to suggest that this difficulty can be eliminated by first calculating a matrix relationship between the pressure and the normal velocity on the boundary surface, and setting the resistive component of the matrix to zero. Material damping due to structural vibrations and acoustic treatments is then included in the analysis in a subsequent step by enforcing specified impedance boundary conditions.

Following Langley's approach, the author's boundary element code was modified to allow the resistive component of the impedance or admittance matrix to be set to zero. Although this technique was effective at eliminating numerical damping, the numerical solution now suffered from obvious numerical artifacts reminiscent of nonexistence/nonuniqueness difficulties over small frequency ranges. Langley did not observe these relatively narrowband discrepancies because his analysis focused on producing accurate damping predictions for a single resonance. A more thorough analysis of the numerical difficulties for boundary element solutions of interior problems was then undertaken to try to develop a formulation that produces more accurate predictions. Rather than trying to derive theorems using matrix or integral equation theory, a familiar example problem will be used to demonstrate the numerical difficulties. This problem can then be used to test other boundary element programs for similar difficulties and to try potential remedies.

## 2. Definition of the example problem and the analytical solution

A simple example problem of a linear duct, considered previously by Suzuki et al. [1] will be used to demonstrate the numerical difficulties for boundary element solutions of interior acoustic problems. The cross-section of the duct is square with dimensions $0.08\,\mathrm{m}\times 0.08\,\mathrm{m}$ and it is 0.34 m long, as shown in Fig. 1. One end of the duct is vibrating as a piston with amplitude $1\,\mathrm{mm\,s^{-1}}$ and the other end is either rigid or has a specified impedance boundary condition. The pressure on the surface of the piston is to be computed as a function of frequency, where the solution is assumed to be time harmonic with $e^{-i\omega t}$ dependence. The sound speed $c$ and density $\rho$ in the fluid are taken to be $340\,\mathrm{m\,s^{-1}}$ and $1.2\,\mathrm{kg\,m^{-3}}$, respectively. The waves in the duct are one dimensional, and the exact solution for the pressure on the piston is given by [9]

$$\hat{p}=\rho c\hat{v}_0\frac{(z/\rho c)\cos(kL)-\mathrm{i}\,\sin(kL)}{\cos(kL)-\mathrm{i}(z/\rho c)\sin(kL)}, \tag{1}$$

where $L$ is the length of the duct, $k$ is the acoustic wavenumber, and $z$ is the specific acoustic impedance at the end of the duct opposite the piston. The $\hat{}$ notation indicates the complex amplitude of a function, as defined by Pierce [9]. For rigid-wall boundary conditions, $z$ goes to infinity, and the pressure field on the piston becomes $\hat{p}=\mathrm{i}\rho c\hat{v}_0\cot(kL)$.

## 3. Definition of the numerical solution

In this paper, the numerical calculations will be performed primarily with the lumped parameter boundary element program written by the author [10–13]. Ref. [10] contains a computer disk with programs implementing the lumped parameter solution. Although the computer program has been modified and

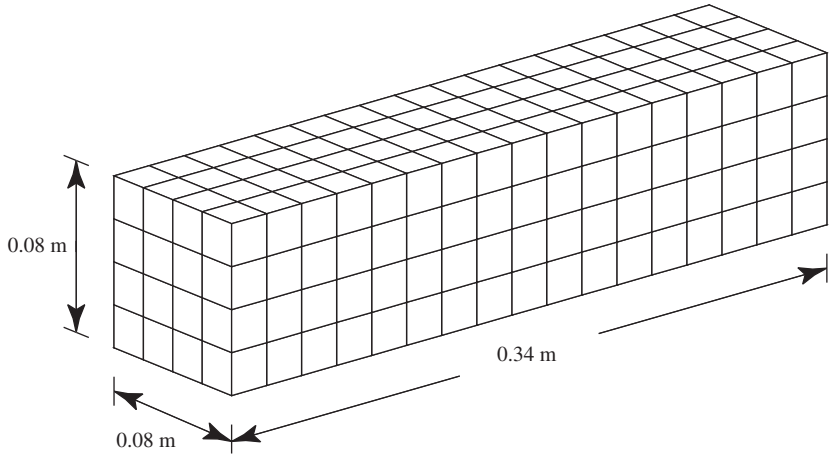


Fig. 1. Definition of the cavity dimensions and illustration of the more refined boundary element mesh with $NA = 304$.

expanded in many ways since the book was published, the basic core subroutines used to compute the coefficient matrices have not changed. In the lumped parameter solution, the pressure field is written in terms of basis functions that satisfy the governing partial differential equation, in this case the Helmholtz equation, throughout the solution domain. The specified boundary condition on the boundary surface of the domain is enforced in a lumped parameter sense over elements. In acoustics, the traditional lumped parameter variables are average pressure, volume velocity, and acoustic impedance. The average pressure and the volume velocity over element $\mu$ can be written, respectively as

$$\hat{p}_\mu = \sum_{v=1}^{NA} \hat{s}_v \left[ \frac{1}{S_\mu} \iint_{S_\mu} b_v(\mathbf{x}) \, \mathrm{d}S(\mathbf{x}) \right], \quad \mu = 1, \ldots, NA \tag{2}$$

and

$$\hat{u}_\mu = \sum_{v=1}^{NA} \hat{s}_v \left[ \frac{1}{\mathrm{i}k\rho c} \iint_{S_\mu} \nabla b_v(\mathbf{x}) \cdot \mathbf{n} \, \mathrm{d}S(\mathbf{x}) \right], \quad \mu = 1, \ldots, NA, \tag{3}$$

where $S_\mu$ is the surface area of element $\mu$, $\hat{s}_v$ is the complex amplitude of basis function $v$, $\mathbf{x}$ is a field point location, $\mathbf{n}$ is the unit surface normal directed into the fluid at $\mathbf{x}$, and $NA$ is the number of acoustic elements. In the subsequent computations using the lumped parameter formulation, the basis functions are taken to be the acoustic pressure fields of discrete sources located at the centers of the acoustic elements. For simple sources, the basis functions are defined as

$$b_v(\mathbf{x}) = \frac{1}{R} \mathrm{e}^{\mathrm{i}kR}, \quad v = 1, \ldots, NA, \tag{4}$$

where $R = |\mathbf{x} - q_v|$, and $q_v$ is the center of element $v$. For dipole sources, the basis functions are defined by

$$b_v(\mathbf{x}) = -\frac{(\mathbf{x} - q_v) \cdot \mathbf{n}_q}{R^3} (\mathrm{i}kR - 1) \mathrm{e}^{\mathrm{i}kR}, \quad v = 1, \ldots, NA, \tag{5}$$

where the dipole source $\mathbf{n}_q$ is aligned with the unit vector pointing normal to the surface and into the fluid at the source location. It is also possible to use hybrid "tripole sources", combining simple and dipole sources with an imaginary coupling coefficient, as basis functions. For exterior radiation problems, tripole sources have been shown to eliminate nonexistence/nonuniqueness difficulties [7], but are not commonly applied to interior problems due to the relatively high computational cost and increased complexity.

In deriving boundary element formulations, one of the more popular approaches is to start from the Kirchhoff–Helmholtz equation, divide the boundary surface into elements, assume the pressure and normal surface velocity is constant over each element, and generate an equation system by collocating the pressure at the center of each of the elements [1,14,15]. The matrices resulting from the conventional approach are very

similar to those produced using discrete sources at the element centers as basis functions with the boundary conditions enforced in a lumped parameter sense. Thus, the numerical calculations using the lumped parameter method should yield results that would be typical for a conventional boundary element analysis. Further confirmation of the similarity of the two numerical solutions is given subsequently.

## 4. Artificial damping in the boundary element solution

Once the representation of the acoustic field is defined, the solution for the pressure field can be determined in a number of ways. The most straightforward method is to derive and solve an equation system for the source amplitudes that enforce the boundary conditions. It is assumed that volume velocity boundary conditions are specified for $NU$ elements, average pressure boundary conditions are specified for $NP$ elements, and acoustic impedance boundary conditions are specified for $NZ$ elements. For volume velocity boundary conditions, equations can be written in terms of the source amplitudes as

$$\hat{u}_\mu = \sum_{\nu=1}^{NA} U_{\mu\nu}\hat{s}_\nu, \quad \mu = 1,\ldots,NU. \tag{6}$$

For average pressure boundary conditions, the equations are

$$\hat{p}_\mu = \sum_{\nu=1}^{NA} P_{\mu\nu}\hat{s}_\nu, \quad \mu = NU+1,\ldots,NU+NP. \tag{7}$$

Using terms from the **P** and **U** matrices, impedance boundary conditions can be directly enforced as

$$\sum_{\nu=1}^{NA}(P_{\mu\nu} - z_\mu U_{\mu\nu})\hat{s}_\nu = 0, \quad \mu = NU+NP+1,\ldots,NA, \tag{8}$$

where $z_\mu$ is the acoustic impedance for element $\mu$. A matrix equation can thus be constructed that enforces the specified boundary condition directly. Solving for the source amplitudes in this way is advantageous because only the cavity resonances for the correct boundary conditions enter into the solution process.

To illustrate the effects of artificial damping for the duct example problem, rigid-wall boundary conditions are assumed at the end of the duct opposite the piston, and the pressure is computed on the surface of the piston at a frequency resolution of 1 Hz. Fig. 2 shows comparisons between the analytical and boundary element solutions using simple sources as basis functions. The boundary element computations were performed for two mesh densities to illustrate the effect of mesh resolution. The more refined mesh corresponds to that in the original paper by Suzuki et al. [1] and the element size in the coarser mesh is approximately twice as large. The boundary element predictions from the paper by Suzuki et al. are superposed in the figure to demonstrate that their solution has approximately the same level of accuracy as that for the refined mesh. Their results are computed at approximately 20 Hz resolution, so that artificial damping near the response peaks is not readily apparent. It is possible to extract equivalent loss factors for

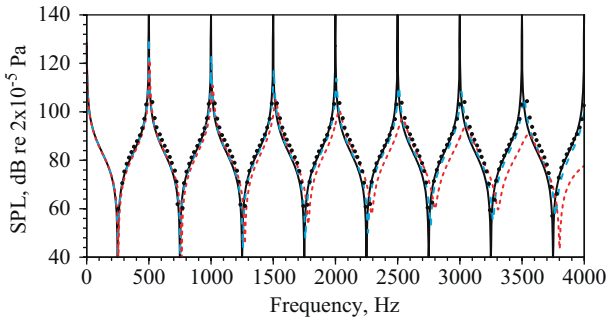


Fig. 2. Pressure on the surface of the piston as a function of frequency computed by directly imposing the boundary conditions (——, analytical; - - - -, $NA = 304$; ·····, $NA = 72$; ●, Suzuki).

each of the modes using a technique similar to that discussed by Fahnline [13]. Fig. 3 shows computed modal loss factors for the lumped parameter computations using simple sources as basis functions. The lines in the figure connect the loss factors for the modes with plane waves along the length of the duct. The results confirm that the artificial damping diminishes with increasing mesh resolution, as discussed previously by Langley [2].

To verify that this numerical difficulty is endemic to all boundary element solutions, several other computer programs were used to solve the same problem, including Sysnoise [16] (Rev. 5.4, direct boundary collocation solution for interior problems), Helm3D [17], and VNoise [18]. These programs were chosen mainly because they were available to the author. The results for the pressure field on the surface of the piston using the coarse surface element mesh are shown in Fig. 4 for each of the boundary element programs. Clearly, all the programs suffer from the same numerical difficulty with artificial damping. The conventional rule-of-thumb is that boundary element solutions are valid as long as the boundary surface is discretized with at least six elements per wavelength. For the coarse element mesh with 72 elements used in the computations, the solutions should be valid to approximately 1400 Hz. All of the numerical solutions show considerable artificial damping below this frequency.

The logical question then is, "If all boundary element solutions have this defect, then why hasn't this difficulty been more thoroughly analyzed?" The likely answer is that artificial damping is not perceived as a problem in practice because all real structural–acoustic systems have some level of damping. Also, as with all boundary element computations, solution accuracy can be ensured by diligently validating results with mesh convergence tests, but at the cost of considerably longer computation times. In a practical situation, artificial damping would be most problematic when acoustic treatments on the walls are included in the analysis. Since both damping mechanisms tend to increase with frequency, it would be hard to discern between them, possibly leading to erroneous predictions of the effectiveness of the acoustic treatments. To illustrate their interaction, the duct example problem was solved with two different impedance boundary conditions specified on the end of the duct opposite the piston. The two values for the specific impedance were taken as $z = 10 + i130.56\,\mathrm{N\,m^{-3}}$ and $z = 96.92 + i130.56\,\mathrm{N\,s\,m^{-3}}$, yielding absorption coefficients (as defined by Pierce

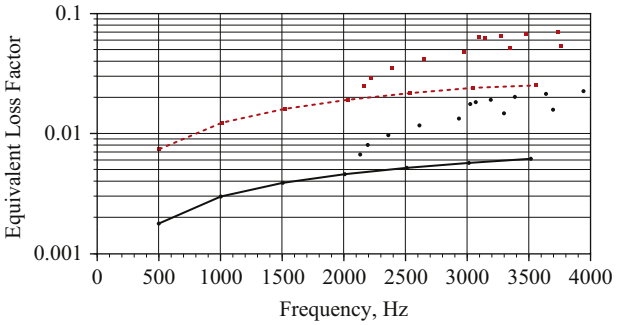


Fig. 3. Equivalent modal loss factors at the interior resonance frequencies for hard-wall boundary conditions (●, $NA = 304$; ——, plane wave modes; ■, $NA = 72$; ·····, plane wave modes).

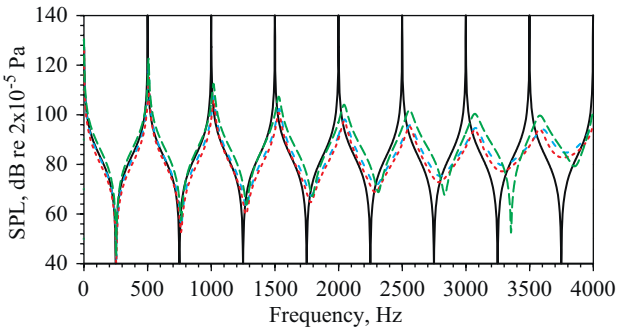


Fig. 4. Pressure on the surface of the piston as a function of frequency (——, analytical; - - - -, Sysnoise; ·····, Helm3D; – – –, VNoise).

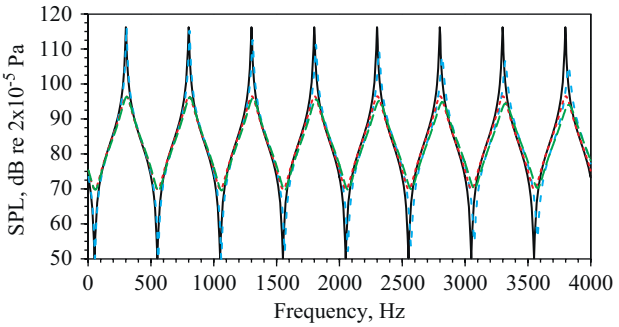


Fig. 5. Pressure on the surface of the piston as a function of frequency computed by directly imposing the boundary conditions ($z = 10 + \mathrm{i}130.56\,\mathrm{N\,s\,m^{-3}}$; ——, analytical; - - - -, $NA = 304$; $z = 96.92 + \mathrm{i}130.56\,\mathrm{N\,s\,m^{-3}}$; ·····, analytical; – – –, $NA = 304$).

[9, p. 109]) of 0.0851 and 0.585, respectively. (Specific acoustic impedances are given because acoustic impedances vary with surface element area.) Fig. 5 shows comparisons of the pressure on the surface of the piston for the analytical and boundary element solutions where the computations were performed using simple sources as basis functions and the more refined surface element mesh. As expected, the error in the boundary element solution is much smaller when the absorption coefficient for the walls is higher.

## 5. Error in matching the specified boundary condition

In the previous section, artificial damping was shown to exist in boundary element solutions of interior problems, and the goal in this section is to explain the cause. In a boundary method, the solution is assumed in terms of functions that satisfy the governing partial differential equation throughout the solution domain. For Laplace's equation, it can be shown that the maximum error in the solution occurs on the boundary surface, and the error can be computed once the solution is known [19]. This is not possible for the Helmholtz equation due to resonance effects. For example, even though the boundary condition satisfied by a numerical solution is only slightly different from that specified, the solution at a field point location can be much more inaccurate if the sets of modes excited by the two boundary conditions are different. However, in broad terms, the solution accuracy is still determined by how well the specified boundary condition is satisfied [20]. In this section, it will be shown that the artificial damping is ultimately related to how well the numerical solution satisfies the specified boundary condition.

In a lumped parameter solution, the boundary conditions are matched over elements and errors occur because the specified boundary condition is not matched on a point-by-point basis. To try to determine the level of error in this approximation, the normal surface velocity over each element in the numerical solution can be divided into a constant component and a component with zero volume velocity as

$$\hat{v}_n(\mathbf{x}) = \hat{u}/S + \hat{v}_{n,0}(\mathbf{x}). \tag{9}$$

The $\hat{u}/S$ term represents the monopole component of the sound radiation from the element, and the $\hat{v}_{n,0}(\boldsymbol{x})$ term contains the higher-order components. Because the elements are assumed to be much smaller than the acoustic wavelength, the monopole term typically dominates the sound radiation, except if the higher-order terms have much larger amplitude. Knowing that it is desirable to force $\hat{v}_{n,0}(\boldsymbol{x})$ to be as small as possible, an indication of the how well the boundary condition is matched in the numerical solution is then given by

$$E = \sum_{\mu=1}^{NA} \iint_{S_\mu} |\hat{v}_{n,0}(\mathbf{x})|\,\mathrm{d}S(\boldsymbol{x}) \Big/ \sum_{\mu=1}^{NA} |\hat{u}_\mu|. \tag{10}$$

Substituting for $\hat{v}_{n,0}(\boldsymbol{x})$ from Eq. (9) and for $\hat{v}_n(\boldsymbol{x})$ in terms of the normal velocity of the basis function yields

$$E = \sum_{\mu=1}^{NA} \iint_{S_\mu} \left| \frac{1}{\mathrm{i}k\rho c} \sum_{\nu=1}^{NA} \hat{s}_\nu \nabla b_\nu(\mathbf{x}) \cdot \mathbf{n} - \frac{\hat{u}_\mu}{S_\mu} \right| \mathrm{d}S(\mathbf{x}) \Big/ \sum_{\mu=1}^{NA} |\hat{u}_\mu|. \tag{11}$$

Unfortunately, it is difficult to evaluate the surface integral in the numerator when $\mu = \nu$ because it is singular, and it would be far easier to perform the calculations if the "self-term" is excluded from the summations. As a reasonable approximation, the contribution from the self-term is assumed to be equal to that of the specified normal surface velocity, such that error in matching the boundary condition reduces to

$$E' \approx \sum_{\mu=1}^{NA} \iint_{S_\mu} \left| \frac{1}{ik\rho c} \sum_{\nu=1,\nu\neq\mu}^{NA} \hat{s}_\nu \nabla b_\nu(\mathbf{x}) \cdot \mathbf{n} \right| dS(\mathbf{x}) \Big/ \sum_{\mu=1}^{NA} |\hat{u}_\mu|. \tag{12}$$

The integrals are now nonsingular and can be accurately performed using standard Gauss quadrature. In simple terms, the error estimate $E'$ computes the variation in the normal velocity over the surface of the elements in comparison to the constant component. It is primarily useful as a way to assess solution error as a function of frequency for a single boundary element mesh. In particular, it is very helpful in diagnosing and explaining the cause of nonuniqueness/nonexistence difficulties.

To illustrate, the duct problem is reconsidered with the element surface normal directions switched so that the sound field is to be computed in the exterior region. For exterior problems, it is well known that when the basis functions are assumed in terms of simple or dipole sources alone, the solution suffers from nonexistence/nonuniqueness difficulties at the resonance frequencies of the interior volume for pressure release and rigid-wall boundary conditions, respectively [7,14]. For hard-wall boundary conditions, acoustic resonances in the interior volume occur for plane wave modes at the frequencies

$$f_\mu = \mu(340\,\mathrm{m\,s^{-1}})/2(0.34\,\mathrm{m}) = \mu(500\,\mathrm{Hz}), \quad \mu = 0, 1, 2, \ldots . \tag{13}$$

For pressure release boundary conditions, the resonances in the frequency range below 4 kHz have a half-wavelength across the cross-section of the duct in both directions. The resonances in the frequency range of interest are thus given by

$$f_\mu = \frac{(340\,\mathrm{m\,s^{-1}})}{2} \sqrt{2[1/(0.08\,\mathrm{m})]^2 + [\mu_x/(0.34\,\mathrm{m})]^2}, \quad \mu = 1, 2, \ldots , \tag{14}$$

where the $x$-axis is along the centerline of the duct, and $\mu = (\mu_x, \mu_y, \mu_z) = (\mu_x, 1, 1)$. For $\mu_x = 1$–5 the resonance frequencies are 3046, 3167, 3359, 3610, and 3909 Hz.

To demonstrate how nonexistence/nonuniqueness difficulties affect solution accuracy, Fig. 6 shows the computed acoustic power output as a function of frequency for the more refined surface element mesh using simple, dipole, and tripole sources as basis functions. For the dipole sources, the solution varies wildly about the correct solution, with a distinct change in phase at the interior resonance frequencies. For simple sources the deviations are much more subtle, and would probably be considered inconsequential for most practical engineering analyses. Unfortunately, the solution errors become much larger as the surface element mesh is refined, but are confined smaller frequency ranges near the interior resonances. Comparing the two sets of frequencies in Eqs. (13) and (14) to the curves in Fig. 6 confirms that the numerical difficulties occur at the interior resonance frequencies.

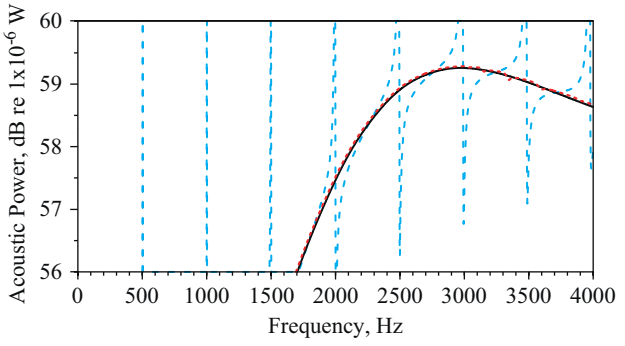


Fig. 6. Computed acoustic power output as a function of frequency for the exterior boundary value problem with $NA = 304$ (——, tripole sources; - - - -, dipole sources; ·····, simple sources).

An explanation for the degradation in solution accuracy is given by the error estimate, as shown in Fig. 7 for each of the source types. The peaks in the error estimate closely correspond to the interior resonance frequencies. Physically, the surface velocity tends to vary wildly at the interior resonance frequencies because source amplitude distributions that create very little volume velocity over any of the surface elements exist. The source amplitudes then become increasingly large as the interior resonance frequencies are approached to try to overcome the large level of cancellation on the boundary surface, ultimately creating a surface velocity distribution with wild variations. As the higher-order component of the surface velocity grows, it eventually overwhelms the monopole component, leading to relatively large errors in the solution. A good example to illustrate this effect is sphere with a uniform source distribution, as discussed previously by Lamb [21] and Schenck [14].

Returning to the interior problem, a similar calculation can be performed when the acoustic field is computed inside the duct. Fig. 8 shows the computed error estimates for the more refined surface element mesh using simple, dipole, and tripole sources as basis functions. The error estimate for the solution using dipole sources is identical to that shown previously in Fig. 7, as is expected since dipole sources produce equal and opposite velocity distributions on the two sides of the boundary surface. For all the source types, the peaks in the error estimate occur near the interior resonance frequencies for hard-wall boundary conditions, and thus the solution accuracy is expected to degrade near these frequencies. For confirmation, Fig. 9 shows predictions for the pressure on the surface of the piston using the different source types. All of the source types yield reasonable predictions, with the largest solution errors near the resonance and anti-resonance frequencies, as expected. For the sake of simplicity, simple sources are used as basis functions for the subsequent computations even though the artificial damping is somewhat smaller near the resonance peaks for the computations using dipole sources. Overall, it is not clear how the error estimate relates to the solution accuracy in an absolute sense, since dipole sources yield the same estimate for interior and exterior problems, but the solution accuracies differ considerably.

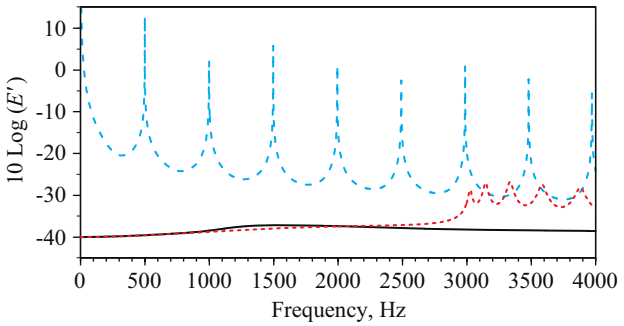


Fig. 7. The estimated error in matching the specified boundary condition as a function of frequency for the exterior boundary value problem with $NA = 304$ (——, tripole sources; - - - -, dipole sources; ·····, simple sources).

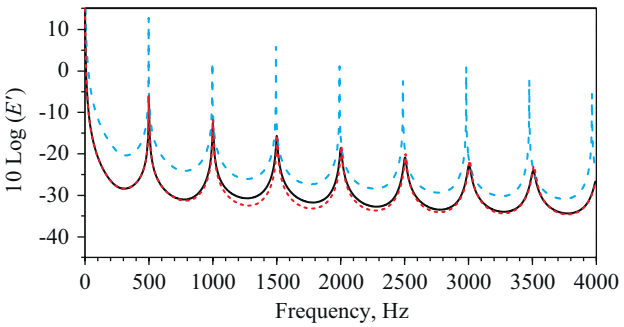


Fig. 8. The estimated error in matching the specified boundary condition as a function of frequency for the interior boundary value problem with $NA = 304$ (——, tripole sources; - - - -, dipole sources; ·····, simple sources).

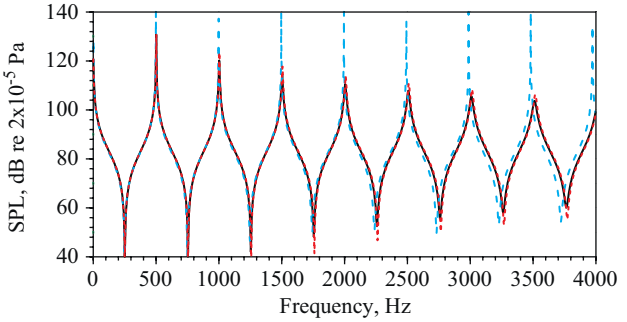


Fig. 9. Pressure on the surface of the piston as a function of frequency for the interior boundary value problem computed by directly imposing the boundary conditions problem with $NA = 304$ (——, tripole sources; - - - -, dipole sources; ·····, simple sources).

Summarizing the results in this section, it has been shown that the error in matching the specified boundary condition is a good indicator for nonexistence/nonuniqueness phenomena. For exterior problems, these difficulties are purely numerical artifacts. Because simple and dipole sources basis functions excite different sets of interior resonances, they can be combined together to yield a hybrid tripole source basis function that does not suffer nonexistence/nonuniqueness difficulties. The situation is different for interior problems. Although the interior resonances are physically meaningful, the actual boundary value problem does not have a unique solution when the homogeneous version of the boundary value problem has a nontrivial solution. It then becomes difficult to match the specified boundary condition near the interior resonance frequencies and the solution error increases. Thus, the cause of the numerical difficulties is essentially the same for interior and exterior problems.

## 6. Solution derived from the impedance matrix

As an alternative to imposing the boundary conditions directly, it is possible to derive a boundary element solution by first computing an acoustic impedance matrix, and then using it to compute the volume velocity vector that enforces the boundary conditions. Using Eqs. (6) and (7), the acoustic impedance matrix relating the volume velocity and the average pressure on the boundary surface is given as $\mathbf{Z} = \mathbf{P}\mathbf{U}^{-1}$. In theory, this matrix should be entirely reactive for an interior problem.

It has been suggested [2] that artificial damping in boundary element solutions can be eliminated by simply setting the resistive component of the impedance matrix to zero. This assumption will be discussed subsequently, but first a simple derivation will be given showing how the impedance matrix can be used to solve problems with pressure and/or impedance boundary conditions. The basic strategy is to rewrite the pressure and impedance boundary conditions in terms of the acoustic impedance matrix and the volume velocity vector. It will then be possible to compute a volume velocity vector which enforces all the boundary conditions simultaneously. To facilitate partitioning the matrix and computing a solution, the acoustic elements are rearranged so that pressure boundary conditions are specified on elements 1 through $NP$, impedance boundary conditions are specified on element $NP+1$ through $NP+NZ$, and volume velocity boundary conditions are specified on elements $NP+NZ+1$ through $NA$. Equations enforcing pressure boundary conditions can be written as

$$\hat{p}_\mu - \sum_{v=NP+NZ+1}^{NA} Z_{\mu v}\hat{u}_v = \sum_{v=1}^{NP+NZ} Z_{\mu v}\hat{u}_v, \quad \mu = 1,\ldots,NP. \tag{15}$$

Since volume velocities are specified for elements $NP+NZ+1$ through $NA$, the second term on the left side of the equation represents a known quantity. Similarly, impedance boundary conditions can be rewritten in terms of the volume velocity vector as

$$-\sum_{v=NP+NZ+1}^{NA} Z_{\mu v}\hat{u}_v = \sum_{v=1}^{NP+NZ} Z_{\mu v}\hat{u}_v - z_\mu\hat{u}_\mu, \quad \mu = NP+1,\ldots,NP+NZ. \tag{16}$$

Taken together, Eqs. (5) and (6) now represent an equation system with $NP+NZ$ unknowns. Solving the system yields the volume velocity vector enforcing all the boundary conditions simultaneously. It is easily verified that this implementation yields identical solutions to the original formulation. However, it is now possible to set the resistive component of the acoustic impedance matrix equal to zero before solving the equation system. Once the volume velocity vector has been determined, the pressure on the boundary surface can be computed in a similar fashion, with the resistive component of the acoustic impedance matrix set to zero.

To test the algorithm, rigid-wall boundary conditions are assumed at the end of the duct opposite the piston, and the pressure is computed on the surface of the piston. Fig. 10 shows comparisons between the analytical and boundary element solutions using simple sources. Clearly, the solution suffers from numerical difficulties at the interior resonance frequencies for hard-wall boundary conditions. Focusing on the resonance peak near 1000 Hz, Fig. 11 shows the breakdown of the pressure over the piston into its resistive and reactive components as computed using Eqs. (6)–(8). The results show that the formulation using the reactive component of the impedance matrix becomes inaccurate when the real component of the pressure field is larger than the imaginary component. In simple terms, neglecting the resistive component of the impedance matrix is not appropriate unless it is much smaller than the reactive component.

As the results in Figs. 10 and 11 show, this formulation is not ideal for problems with normal surface velocity boundary conditions, because the interior resonances occur at the frequencies where the error in the impedance matrix is the largest. The solution is much more promising when other boundary conditions are imposed and the two sets of resonance frequencies are different. To illustrate, Fig. 12 shows the analytical solution and numerical predictions for the pressure on the piston for the two impedance boundary conditions considered previously. Compared to the previous results in Fig. 5, the damping is now predicted much more accurately over the entire frequency range. Unfortunately, the solution still diverges at the interior resonance frequencies for hard-wall boundary conditions. The results imply that zeroing out the resistive component is effective in reducing artificial damping, but errors still exist in the reactive component of the acoustic

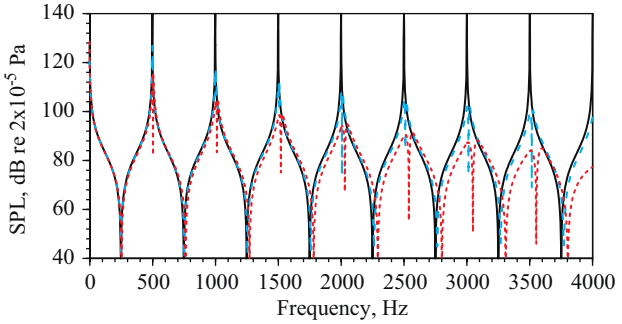


Fig. 10. Pressure on the surface of the piston as a function of frequency computed using the reactive component of the acoustic impedance matrix (——, analytical; - - - -, $NA = 304$; ·····, $NA = 72$).

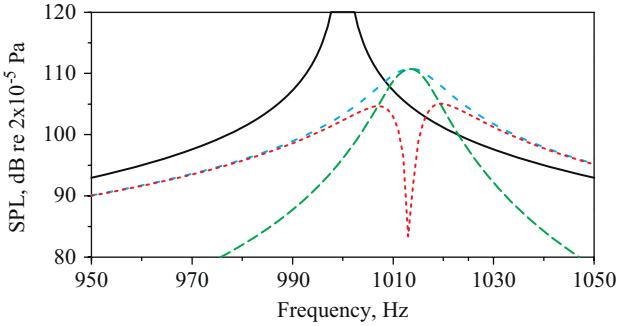


Fig. 11. Pressure on the surface of the piston as a function of frequency computed by directly imposing the boundary conditions (——, analytical; - - - -, $|\hat{p}|$; ·····, $|\mathrm{Im}\{\hat{p}\}|$; – – –, $|\mathrm{Re}\{\hat{p}\}|$).

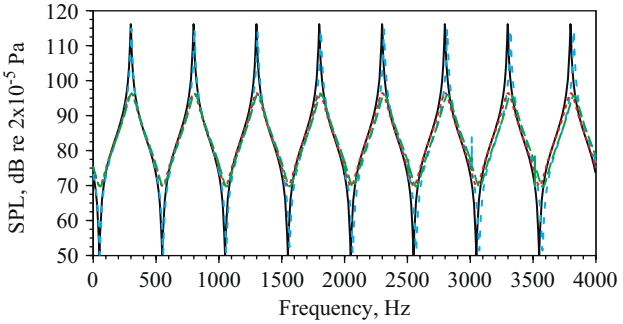


Fig. 12. Pressure on the surface of the piston as a function of frequency computed using the reactive component of the acoustic impedance matrix ($z = 10 + i130.56\,\mathrm{N\,s\,m^{-3}}$; ——, analytical; - - - -, $NA = 304$; $z = 96.92 + i130.56\,\mathrm{N\,s\,m^{-3}}$; ·····, analytical; – – –, $NA = 304$).

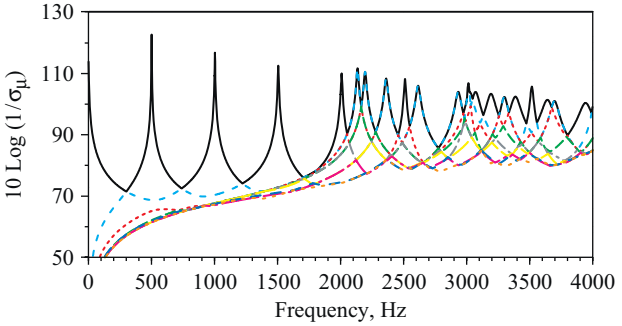


Fig. 13. Reciprocal of the singular values of the matrix **U** as a function of frequency (——, $\sigma_1$; - - - -, $\sigma_2$; ·····, $\sigma_3$; – – –, $\sigma_4$; – · –, $\sigma_5$; ——, $\sigma_6$; – · – –, $\sigma_7$; – –, $\sigma_8$; · · · · ·, $\sigma_9$).

impedance matrix. An impedance formulation is used in the papers by Bernhard et al. [22], Hussain and Peat [23], and Sorokin and Christensen [24], thus explaining the numerical difficulties they experienced, particularly at very low frequencies where a resonance exists for hard-wall boundary conditions. Since the associated mode shape is constant throughout the interior volume, it is expected that it will be difficult to match the constant component of the pressure field at low frequencies.

Integral equation theory can be used to explain why the numerical solution is inaccurate at the interior resonance frequencies for hard-wall boundary conditions. Only a cursory explanation will be given here, and a more detailed derivation of the theory can be found in the books by Filippi et al. [7] and Hildebrand [8]. In deriving the acoustic impedance matrix, **U** is inverted, which relates elemental volume velocities to source amplitudes. It cannot be inverted if a set of source amplitudes that produce zero volume velocities over each of the elements simultaneously exist, since the source amplitudes can be added to the solution with arbitrary amplitude without changing the resulting volume velocity vector. In mathematical terms, the solution is not unique. In the present application, the homogeneous equation has a nontrivial solution near the interior resonance frequencies for hard-wall boundary conditions, and thus causes the matrix inversion to become unstable. To illustrate, Fig. 13 shows the reciprocal of the singular values of **U** as a function of frequency using simple sources as basis functions and the more refined surface element mesh. The peaks in the plot correspond to minimums in the singular values, and closely match the frequencies where the formulation using the reactive component of the impedance matrix experiences "dropouts". Thus, the singular value decomposition can be used to determine the frequencies where the matrix inversion is unstable.

## 7. Solution derived from the admittance matrix

Instead of computing an acoustic impedance matrix, an acoustic admittance matrix relating volume velocity to pressure can be computed as $\mathbf{A} = \mathbf{U}\mathbf{P}^{-1}$. Since the matrix **P** is inverted rather than **U**, and it relates average

pressures to source amplitudes, the admittance matrix will suffer from nonexistence/nonuniqueness difficulties at the interior resonance frequencies for pressure release boundary conditions. Initially, trading one set of resonance frequencies for another does not seem particularly advantageous. Upon closer inspection though, the resonance frequencies for pressure release boundary conditions are preferable because they do not begin until the smallest dimension of the boundary surface is at least one half the acoustic wavelength. This can be demonstrated by plotting the reciprocal of the singular values of **P** as a function of frequency, as shown in Fig. 14. Again, the peaks in the plot correspond to minimums in the singular values. Thus, there is no "rigid body" mode at 0 Hz and there are no modes with constant pressure across a cross-section of the boundary surface.

As for the impedance matrix, the admittance matrix can be used to derive a solution for arbitrary boundary conditions. Only now the solution is written for the pressure vector instead of the volume velocity vector. Rearranging the order of the terms of the matrix, the elements with volume velocity and impedance boundary conditions are assumed to be numbered $1, \ldots, NU$, and $NU+1, \ldots, NU+NZ$, respectively. The equation system now becomes

$$\hat{u}_\mu - \sum_{v=NU+NZ+1}^{NA} A_{\mu v}\hat{p}_v = \sum_{v=1}^{NU+NZ} A_{\mu v}\hat{p}_v, \quad \mu = 1, \ldots, NU \tag{17}$$

and

$$-\sum_{v=NU+NZ+1}^{NA} A_{\mu v}\hat{p}_v = \sum_{v=1}^{NU+NZ} A_{\mu v}\hat{p}_v - \frac{\hat{p}_\mu}{z_\mu}, \quad \mu = NU+1, \ldots, NU+NZ. \tag{18}$$

There are now $NU+NZ$ equations and unknowns, with the pressure specified on elements $NU+NZ+1, \ldots, NA$. As in the previous section, this formulation allows the resistive component of the admittance matrix to be set to zero for interior problems.

To test the algorithm, rigid-wall boundary conditions are assumed at the end of the duct opposite the piston, and the pressure is computed on the surface of the piston. Fig. 15 shows comparisons between the analytical and boundary element solutions using simple sources. Clearly, the solution is much more accurate than either of the previous solutions shown in Figs. 2 and 10. As expected, the inversion of **P** becomes unstable at the interior resonance frequencies for pressure release boundary conditions, although these defects are only barely visible in the solution for the finer mesh resolution. Aside from producing much more accurate predictions, the admittance matrix is also much easier to interpolate at low frequencies due to the absence of interior resonances. Thus, fewer "master frequencies" are required to define the admittance matrix's functional dependence.

In Section 3, it was stated that the lumped parameter model produces matrices similar to those generated using a conventional boundary element approach. One way to demonstrate that they are alike is to compare their singular values as a function of frequency. Matrices comparable to **P** and **U** can be generated using the conventional boundary element program Helm3D, which is described in the book edited by Wu [17]. Eq. (14) of Chapter 3 gives a relationship between pressure and normal velocity over the surface elements, from which

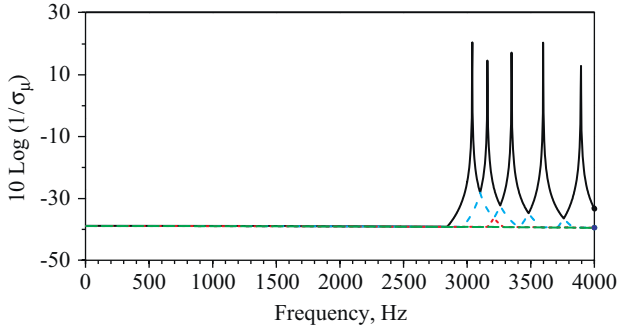


Fig. 14. Reciprocal of the singular values of the matrix **P** as a function of frequency (——, $\sigma_1$; - - - -, $\sigma_2$; ·····, $\sigma_3$; – – –, $\sigma_4$).

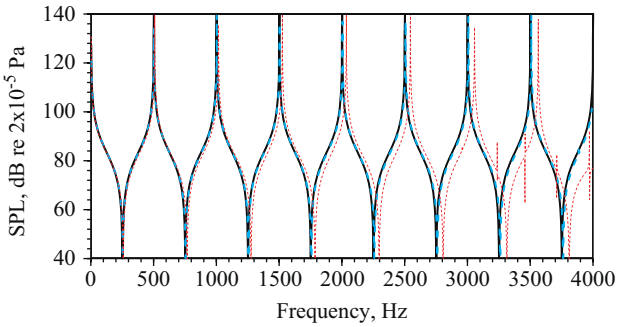


Fig. 15. Pressure on the surface of the piston as a function of frequency computed using the reactive component of the acoustic admittance matrix (——, analytical; - - - -, $NA = 304$; ·····, $NA = 72$).

it can be concluded that the matrices **H** and **G** should be very similar to **P** and **U**, respectively. Indeed, the singular values of the two sets of matrices are very similar, giving further confirmation that the lumped parameter model produces matrices that are very similar to those for conventional boundary element models.

## 8. Summary and conclusions

In this paper, an example problem was used to demonstrate numerical difficulties experienced when solving interior acoustic problems using boundary element methods. It was shown that if the equation system is written in terms of the specified boundary conditions directly, the solution suffers from artificial damping, which was shown to be related to errors in matching the specified boundary condition on a point-by-point basis. As originally suggested by Langley [2], this problem is alleviated if the numerical implementation is reformulated in terms of the reactive component of either the acoustic admittance or impedance matrix. However, the more thorough analysis given here has shown that the solution instead suffers from nonexistence/nonuniqueness difficulties at the interior resonances for either pressure release (admittance formulation) or hard-wall (impedance formulation) boundary conditions. It was also shown that the nonexistence/nonuniqueness difficulties can be detected by plotting the singular values of the matrix that is inverted in process of generating the admittance or impedance matrix, and searching for frequencies where one of the singular values undergoes a minimum. Of the three methods used to derive boundary element solutions for interior problems, the overall accuracy is much higher using the reactive component of the admittance matrix. This advantage is more pronounced for boundary element analyses of ducts and mufflers where the cross-sectional dimensions are small compared to the other dimensions, such that nonexistence/nonuniqueness difficulties do not occur until relatively high frequency.

One of the primary motivations for writing this paper was to alert the boundary element community to these numerical difficulties, so that collectively a remedy might be discovered. Although not discussed in the paper, the author has tried numerous techniques to address the difficulties. Since the formulations using the impedance and admittance matrices suffer from nonexistence/nonuniqueness difficulties at different sets of frequencies, perhaps they can be combined together to yield an accurate solution over the entire frequency range, much in the same way that simple and dipole sources are combined for exterior radiation problems using the Burton and Miller technique [25]. However, it may not be possible since the impedance and admittance matrices are inverses of each other, and have the same information. Presently, the author has not been able to derive such a formulation. It would also be possible to partition the acoustic matrices such that the matrix relating pressure to volume velocity is written in terms of mixed variables. The nonexistence/nonuniqueness difficulties would then occur at the interior resonance frequencies for a combination of pressure release and hard-wall boundary conditions. This might conceivably increase the fundamental resonance frequency and provide a larger low-frequency range without nonexistence/nonuniqueness difficulties. However, it is expected that pressure release boundary conditions already produce the largest fundamental resonance frequency. Unfortunately, the number of possible combinations of the pressure and volume velocity boundary conditions goes as $NA!$, so that it is impractical to try to demonstrate by brute force

that pressure release boundary conditions produce the highest fundamental frequency for any but the smallest problems. Ultimately, the formulation using the reactive component of the admittance yields accurate solutions for many problems, but it would be desirable to reformulate the solution such that its accuracy deteriorates slowly with increasing frequency, similar to the way the Burton and Miller formulation performs for boundary element solutions of exterior problems.

## References


[1] S. Suzuki, S. Maruyama, H. Ido, Boundary element analysis of cavity noise problems with complicated boundary conditions, *Journal of Sound and Vibration* 130 (1989) 79–96.

[2] R.S. Langley, A dynamic stiffness/boundary element method for the prediction of interior noise levels, *Journal of Sound and Vibration* 163 (1993) 207–230.

[3] T.W. Wu, P. Zhang, C.Y.R. Cheng, Boundary element analysis of mufflers with an improved method for deriving the four-pole parameters, *Journal of Sound and Vibration* 217 (1998) 767–779.

[4] T.W. Wu, C.Y.R. Cheng, P. Zhang, A direct mixed-body boundary element method for packed silencers, *Journal of the Acoustical Society of America* 111 (2002) 2566–2572.

[5] A. Selamet, I.J. Lee, N.T. Huff, Acoustic attenuation of hybrid silencers, *Journal of Sound and Vibration* 262 (2003) 509–527.

[6] A. Selamet, P.M. Radavich, The effect of length on the acoustic attenuation performance of concentric expansion chambers: an analytical, computational and experimental investigation, *Journal of Sound and Vibration* 201 (1997) 407–426.

[7] P. Filippi, D. Habault, J.P. Lefebvre, A. Bergassoli, *Acoustics: Basic Physics, Theory and Methods*, Academic Press, New York, 1999.

[8] F.B. Hildebrand, *Methods of Applied Mathematics*, second ed., Dover, New York, 1965.

[9] A.D. Pierce, *Acoustics: an Introduction to its Physical Principles and Applications*, Acoustical Society of America, Woodbury, New York, 1989.

[10] G.H. Koopmann, J.B. Fahnline, *Designing Quiet Structures: a Sound Power Minimization Approach*, Academic Press, New York, 1997.

[11] J.B. Fahnline, G.H. Koopmann, A lumped parameter model for the acoustic power output of a vibrating structure, *Journal of the Acoustical Society of America* 100 (1996) 3539–3547.

[12] J.B. Fahnline, G.H. Koopmann, Numerical implementation of the lumped parameter model for the acoustic power output of a vibrating structure, *Journal of the Acoustical Society of America* 102 (1997) 179–192.

[13] J.B. Fahnline, Computing fluid-coupled resonance frequencies, mode shapes and damping loss factors using the singular value decomposition, *Journal of the Acoustical Society of America* 115 (2004) 1474–1482.

[14] H.A. Schenck, Improved integral formulation for acoustic radiation problems, *Journal of the Acoustical Society of America* 44 (1968) 41–58.

[15] D.T. Wilton, Acoustic radiation and scattering from elastic structures, *International Journal for Numerical Methods in Engineering* 13 (1978) 123–138.

[16] Sysnoise Rev. 5.4 User's Manual, *LMS Numerical Technologies*, Leuven, Belgium, 1999.

[17] T.W. Wu (Ed.), *Boundary Element Acoustics: Fundamentals and Computer Codes*, Wit Press, Boston, 2000.

[18] VNoise Node-Limited Demonstration Version, 〈http://www.sts-soft.com/VNoise.aspx〉.

[19] L. Collatz, *The Numerical Treatment of Differential Equations* (P.G. Williams, trans.), third ed., Springer, New York, 1960.

[20] J.B. Fahnline, The External Source Method for the Computation of Acoustic Fields, PhD Thesis, The Pennsylvania State University, 1992.

[21] H. Lamb, *Hydrodynamics*, sixth ed., Dover, New York, 1945.

[22] R.J. Bernhard, B.K. Gardner, C.G. Mollo, C.R. Kipp, Prediction of sound fields in cavities using boundary-element methods, *American Institute of Aeronautics and Astronautics Journal* 25 (1987) 1176–1183.

[23] K.A. Hussain, K.S. Peat, Boundary element analysis of low frequency cavity acoustical problems, *Journal of Sound and Vibration* 169 (1994) 197–209.

[24] S. Sorokin, S.T. Christensen, Low frequency breakdown of boundary element formulation for closed cavities in excitation conditions with a ''breathing''-type component, *Communications in Numerical Methods in Engineering* 16 (2000) 325–334.

[25] A.J. Burton, G.F. Miller, The application of integral equation methods to the numerical solution of some exterior boundary-value problems, *Proceedings of the Royal Society of London Series A* 323 (1971) 201–210.